

# Preparation and Thermophysical Investigations of CoFe<sub>2</sub>O<sub>4</sub>-based Nanofluid: a Potential Heat Transfer Agent

Original Paper Published: 11 May 2018

Volume 32, pages 341–351, (2019) [Cite this article](#)

[Download PDF](#) ↓

Access provided by Dr. Babasaheb Ambedkar Marathwada University, Aurangabad



## [Journal of Superconductivity and Novel Magnetism](#)

[Aims and scope](#)

[Submit manuscript](#)

[Prashant B. Kharat](#) , [Jitendra S. Kounsalye](#), [Mahendra V. Shisode](#) & [K. M. Jadhav](#)

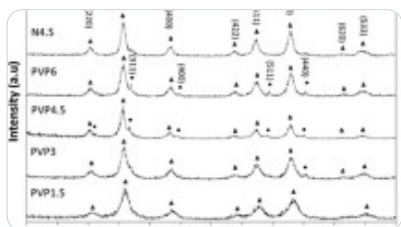
 519 Accesses  17 Citations [Explore all metrics](#) →

## Abstract

Cobalt ferrite nanoparticles were synthesized by employing chemical co-precipitation technique. The structure, morphology, elemental composition, and magnetization studies of cobalt ferrite nanoparticles were carried by XRD, FE-SEM, EDS, and VSM techniques, respectively. Rietveld refined XRD pattern exhibited the single-phase cubic spinel structure

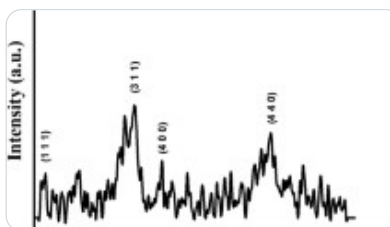
with Fd-3m space group. FE-SEM images indicated some agglomeration of spherical grains which can be attributed to high surface energy and magnetic interactions. Presence of peaks of respective elements (Co, Fe, and O) in EDS spectrum showed formation of CoFe<sub>2</sub>O<sub>4</sub>. The M-H loop recorded at 300 K revealed superparamagnetic behavior and explained by fine particles size. The blocking temperature of the CoFe<sub>2</sub>O<sub>4</sub> nanoparticles from FC-ZFC curve was found to be 144 K. Cobalt ferrite-ethylene glycol nanofluids of various concentrations 0.0–1.0% in steps of 0.2% were prepared by ultrasonically assisted two-step technique. Thermophysical parameters such as thermal conductivity, specific heat, viscosity, and density were investigated as a function of both volume fraction and temperature. The experimental and theoretical value of each sample was correlated. The thermal conductivity was significantly enhanced with an increase in volume fraction and temperature.

## Similar content being viewed by others



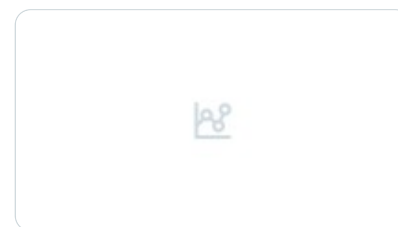
[Phase constituents and magnetic properties of the CoFe<sub>2</sub>O<sub>4</sub> nanoparticles prepared ...](#)

Article | 19 August 2016



[A critical study on the magnetic properties of ultrafine cobalt ferrite nanoparticles...](#)

Article | 02 January 2020



[Structural, magnetic, and acidic properties of cobalt ferrite nanoparticles synthesised by wet...](#)

Article | Open access  
04 July 2015

[Use our pre-submission checklist →](#)

Avoid common mistakes on your manuscript.



## 1 Introduction

Nanofluid consists of solid nanoparticles suspended in a carrier liquid such as water, oil,

polyethylene glycol, and ethylene glycol. Nanofluids were initiated to have several attractive applications [[1,2,3,4,5,6,7,8,9,10,11, 13,14,15](#)], few of them are heating, ventilation, air conditioning and cooling [[6](#)], solar cells [[7](#)], sensor [[4](#)], etc. Typically, water, oil, and ethylene glycol possess low heat transfer capacities than the nanoparticles of Ag, Cu, CuO, Fe<sub>2</sub>O<sub>3</sub>, SiO<sub>2</sub>, CoFe<sub>2</sub>O<sub>4</sub>, NiFe<sub>2</sub>O<sub>4</sub>, etc. with notable thermal conductivity. Spinel ferrite nanoparticles proved its potential use in nanofluid due to its robust nature [[8](#)]. Among carrier liquids, the low freezing point, high boiling point, and moderate heat transfer properties of ethylene glycol motivates its use as the carrier fluid in nanofluids [[9](#)]. Thus, the heat transfer capacities of nanofluids significantly depend on thermal conductivity of nanoparticles suspended in base fluid. Besides excellent magnetic properties, thermal and heat transfer properties of cobalt ferrite (CoFe<sub>2</sub>O<sub>4</sub>) nanoparticles make it a potential material to augment the thermophysical properties of the nanofluid [[10](#)].

The heat transfer and its augmentation studies on CoFe<sub>2</sub>O<sub>4</sub> and ethylene glycol-based nanofluids are described using useful medium theory (EMT) which is based on Maxwell's mean field theory. The reports on thermal conductivity augmentations are within [[11](#)] or beyond [[12](#)] the estimates of useful medium theory. Pastoriza-Gallego et al. [[13](#)], presented the thermal conductivity augmentation of Al<sub>2</sub>O<sub>3</sub>-ethylene glycol nanofluid with both increases of particle concentration as well as temperature and the obtained values are over predicated values. Whereas his other work [[14](#)] reported that the thermal conductivity values are within estimated values for ethylene glycol-based Fe<sub>2</sub>O<sub>3</sub> and Fe<sub>3</sub>O<sub>4</sub> nanofluids. Zhu et al. [[15](#)] revealed that the available models in published studies underestimated the measured thermal conductivities of Fe<sub>3</sub>O<sub>4</sub> aqueous nanofluid and observed that Fe<sub>3</sub>O<sub>4</sub> nanofluids provided more excellent thermal conductivity compared to other nanofluids. Abareshi et al. [[16](#)] showed 11.5% rise in thermal conductivity by addition of 3 volume percent of Fe<sub>3</sub>O<sub>4</sub> nanoparticles at 40 °C. Sundar et al. [[17, 18](#)] interpreted that the Brownian motion of nanoparticles was the main effective parameter to lead the augmentation of thermal conductivity. They developed a new correlation for thermal conductivity prediction regarding concentration along with the temperature. The effect of nanofluid concentration on thermal conductivity of Fe<sub>3</sub>O<sub>4</sub>/water nanofluid was evaluated by Bahiraei and Hangi [[19](#)] and a nonlinear relationship was observed. They suggested the implementation of the neural network to predict the experimental results based on temperature and concentration. Moreover, Bahiraei [[20](#)] examined the migration of particles in Fe<sub>3</sub>O<sub>4</sub>/water nanofluid and

revealed that non-uniform distribution of thermal conductivity could be observed under non-uniformity of nanofluid concentration. From literature survey, it is clear that the thermal conductivity of nanofluids highly depends on the size, shape, and clustering of nanoparticles. Despite numerous studies [21, 22], the exact mechanism responsible for thermal conductivity augmentation remained uncertain because of the lack of molecular-level understanding of the ultrafine particle which demands the systematic studies on the molecular interactions of nanofluids at various concentrations and temperatures.

In the present work, the stable and homogeneous suspensions of CoFe<sub>2</sub>O<sub>4</sub> nanoparticles in ethylene glycol with different volume fractions were prepared. A deep understanding of interactions of ferrite nanoparticles–fluid as a function of concentration and temperature is the primary concern of the present work. The synthesis, characterization of cobalt ferrite nanoparticles, and investigation of thermophysical properties as well as validation with theoretical models of CoFe<sub>2</sub>O<sub>4</sub>–ethylene glycol nanofluids are focused here. Moreover, it is intended to formulate a relationship between thermophysical properties and concentration of CoFe<sub>2</sub>O<sub>4</sub> nanoparticles in nanofluids.

## 2 Materials and Methods

---

### 2.1 Materials

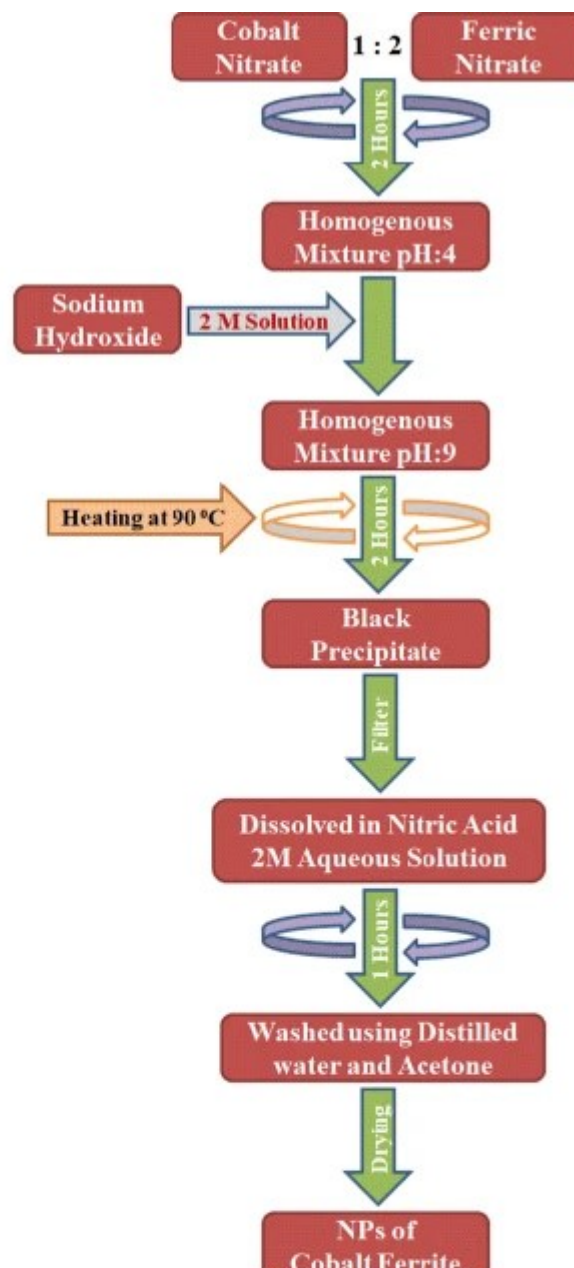
The raw materials to synthesize the cobalt ferrite nanoparticles as cobalt nitrate (Co(NO<sub>3</sub>)<sub>2</sub>·6H<sub>2</sub>O), ferric nitrate (Fe(NO<sub>3</sub>)<sub>3</sub>·9H<sub>2</sub>O), sodium hydroxide (NaOH), and distilled water (H<sub>2</sub>O) were used. Moreover, acetone ((CH<sub>3</sub>)<sub>2</sub>CO) and nitric acid (HNO<sub>3</sub>) is used for impurity removal of the precipitate, if any. Furthermore, ethylene glycol (C<sub>2</sub>H<sub>6</sub>O<sub>2</sub>) was employed to prepare nanofluid. All raw materials were procured by Merck of analytical reagent (AR) grade and used as supplied without any further purification.

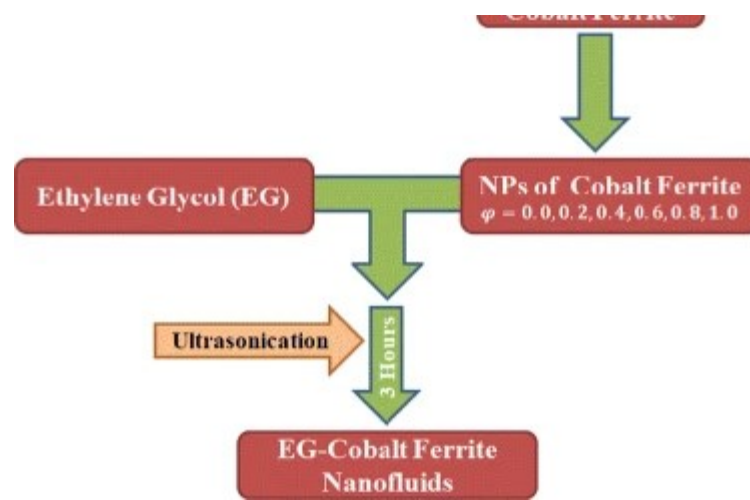
### 2.2 Synthesis

Cobalt ferrite nanoparticles were synthesized using co-precipitation wet chemical technique [23, 24]. The weighed amount of nitrates of respective sources was dissolved in distilled water separately in the stoichiometric ratio as 1:2 (cobalt nitrate/ferric nitrate). The solutions of both nitrates were mixed and stirred to get a homogeneous mixture [8]. The pH of the mixed

solution was adjusted at 9 by adding 2-M sodium hydroxide solution drop by drop. The obtained black precipitate was heated at 90 °C for 2 h and was allowed to cool. Then, it was washed several times with distilled water to remove impurities. An aqueous solution of 2-M nitric acid was added to the precipitate and stirred for 1 h. The supernatant solution was removed, and the residue was cleaned using distilled water and acetone [23]. CoFe<sub>2</sub>O<sub>4</sub> nanoparticles were dispersed in ethylene glycol by employing ultrasonication for 3 h to get a homogenous suspension without any phase separation and sedimentation. The nanofluids of varying volume fraction as 0.0, 0.2, 0.4, 0.6, 0.8, and 1.0% were prepared. A detailed flowchart of synthesis and preparation of cobalt ferrite–ethylene glycol nanofluid is shown in Fig. 1.

Fig. 1





Flowchart of synthesis and preparation of cobalt ferrite–ethylene glycol nanofluid

## 2.3 Characterizations

The structural analysis of CoFe<sub>2</sub>O<sub>4</sub> nanoparticles was carried out by x-ray diffraction (XRD) technique. XRD pattern of CoFe<sub>2</sub>O<sub>4</sub> nanoparticles were obtained using x-ray diffractometer in the  $2\theta$  range of  $20-80^\circ$  with Cu-K $\alpha$  radiation ( $\lambda = 1.506 \text{ \AA}$ ). The Rietveld refinement of XRD pattern was performed using FullProf program. The surface morphology and elemental composition of CoFe<sub>2</sub>O<sub>4</sub> nanoparticles were examined by field emission scanning electron microscope (FE-SEM) equipped with energy-dispersive spectroscopy (EDS) unit, respectively. Magnetic investigations of CoFe<sub>2</sub>O<sub>4</sub> nanoparticles were carried out using vibrating sample magnetometer at room temperature with applied field  $\pm 2$  T. Field-cooled (FC) and zero-field-cooled (ZFC) curves were obtained by superconducting quantum interference device (SQUID) at a field of 100 Oe to study the low-temperature magnetization behavior. The thermophysical parameters such as thermal conductivity, specific heat capacity, density, and viscosity of CoFe<sub>2</sub>O<sub>4</sub>–ethylene glycol nanofluid were measured by KD2 Pro - Decagon Devices, DSC-60 (Shimadzu Corporation), Anton-Paar portable density meter, and viscometer (Brookfield DV-III), respectively.

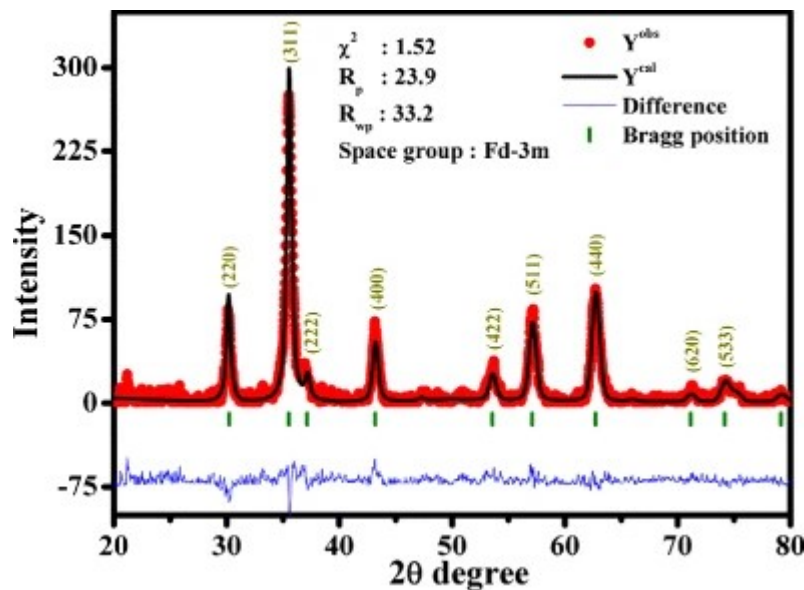
## 3 Results and Discussion

### 3.1 Structure, Morphology, and Magnetic Investigations

### 3.1.1 X-ray Diffraction and Rietveld Refinement

The x-ray diffraction and Rietveld refined XRD pattern of CoFe<sub>2</sub>O<sub>4</sub> is presented in Fig. 2. In Fig. 2, the red line shows observed x-ray diffraction pattern, the black line represents calculated Rietveld refined pattern, and the blue line shows the difference between x-ray diffraction and Rietveld refined pattern of the cobalt ferrite nanoparticles. Green bars show the Bragg's position for the cobalt ferrite nanoparticles.

Fig. 2



X-ray diffraction and Rietveld refined pattern of cobalt ferrite nanoparticles

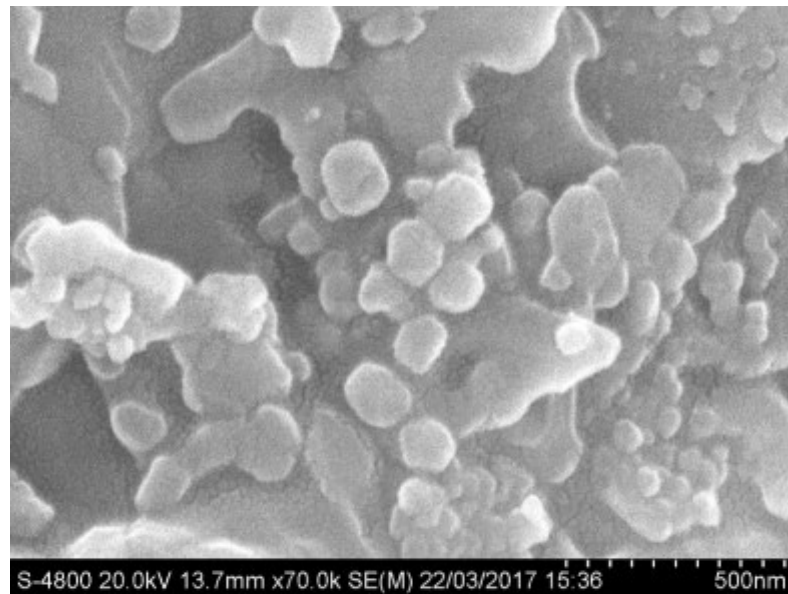
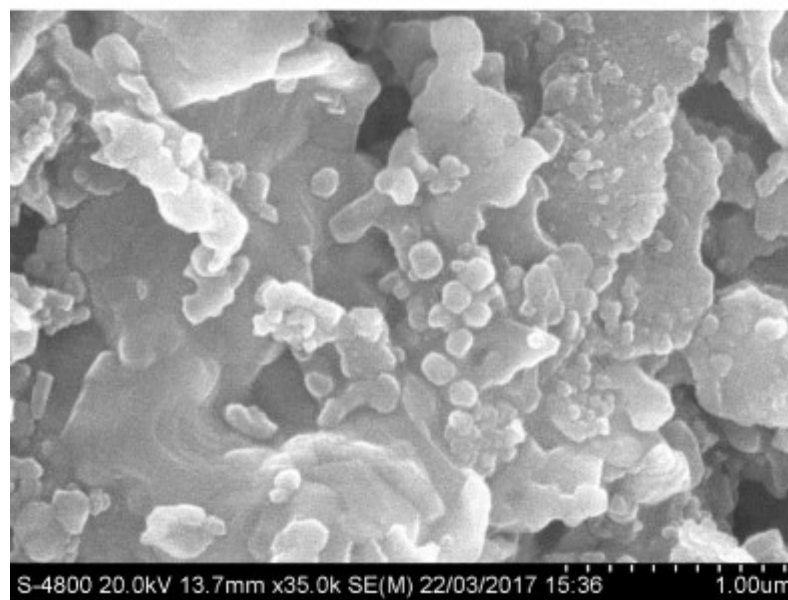
It shows the reflections as (200), (311), (222), (400), (422), (511), (440), (620), and (533) correspond to cubic spinel structure. It exhibits the Fd-3m space group [25, 26]. The experimental pattern match well with that of calculated as well as JCPDS number 96-591-0064. Rietveld refinement parameters as the goodness of fit ( $\chi^2$ ), profile reliability index ( $R_p$ ), and weighted profile reliability index ( $R_{wp}$ ) [27] are presented in Fig. 1. The broad peaks in XRD pattern indicate the fine particle nature and sufficiently small crystallite size. The highest intensity peak (311) was used to estimate the average crystallite size using Scherrer's formula [28] and found to be 11 nm. The lattice parameter  $a$  and x-ray density [29]  $\rho$  obtained from XRD data were found to be 8.374 Å and 537 kg/m<sup>3</sup>, respectively.

### 3.1.2 FE-SEM and EDS

The FE-SEM images of the CoFe<sub>2</sub>O<sub>4</sub> sample are depicted in Fig. [3a, b](#). This figure shows the distribution of particle size is almost homogeneous and the average grain size are below 12 nm, confirming the nanocrystalline nature. Also, the agglomerations of nanoparticles were observed which may be attributed to the high surface energy and magnetic interactions of CoFe<sub>2</sub>O<sub>4</sub> nanoparticles [[30](#)].



Fig. 3

**(a) FE-SEM images of cobalt ferrite nanoparticles.****(b) FE-SEM images of cobalt ferrite nanoparticles.**

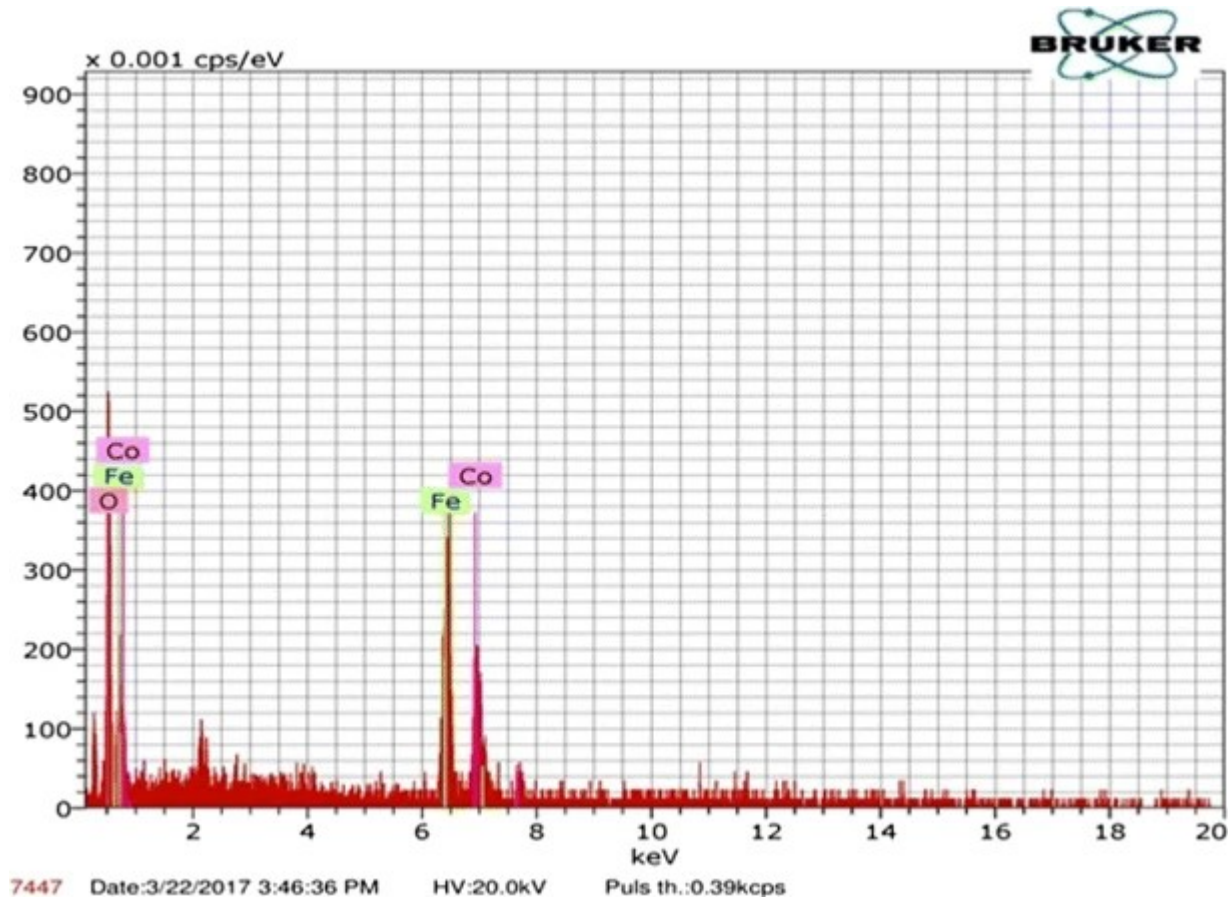
a FE-SEM images of cobalt ferrite nanoparticles. b FE-SEM images of cobalt ferrite nanoparticles

Morphology, particle size, and surface structure of nanoparticles may crucially depend on reaction conditions such as temperature, pH, and calcination temperature. It is reported that the pH of the precursors influences the morphologies of the nanoparticles in co-precipitation method [31]. The pH of the solvent is decreased with an increase in the concentration of

dopants. Subsequently, high amounts of the agent (NaOH) are required to reach the suitable pH of the precipitation [30]. Therefore, the nucleation rate of precipitation and the morphology of nanoparticles may vary from one sample to another. Similar observations were reported [32] for nanocrystalline mixed spinel ferrite prepared using the wet chemical route. The specific surface *S* area was found 98 m<sup>2</sup>/g.

Figure 4 shows EDS spectrum of CoFe<sub>2</sub>O<sub>4</sub> nanoparticles. The elemental composition of CoFe<sub>2</sub>O<sub>4</sub> sample was quantitatively obtained from EDS spectrum. An EDS spectrum indicates the presence of peaks for Co, Fe, and O with no further impurity peak. The obtained atomic ratio of Co, Fe, and O match well with that of expected and maintains the stoichiometric proportion. It is worth mentioning here that the co-precipitation technique and the subsequent heat treatment highly favored the formation of the nanocrystalline CoFe<sub>2</sub>O<sub>4</sub> sample.

Fig. 4



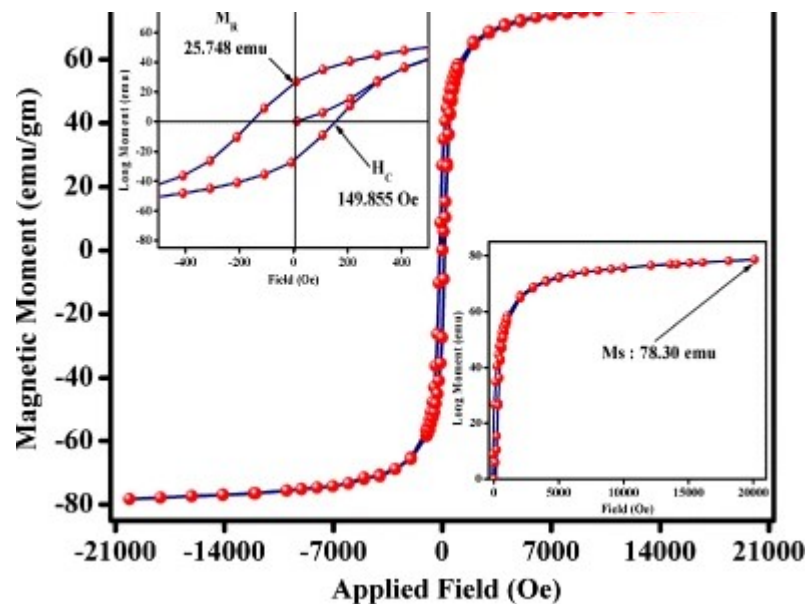
EDS spectrum of cobalt ferrite nanoparticles

### 3.1.3 Magnetization

Magnetization versus applied magnetic field ( $M-H$ ) hysteresis loop of  $\text{CoFe}_2\text{O}_4$  nanoparticles was recorded at 300 K using VSM and presented in Fig. 5.  $M-H$  plot shows that the magnetic anisotropy and magnetic moment per atom of cobalt ferrite nanoparticles is enhanced than those of their bulk form [33]. It is well recognized that a ferromagnetic material in bulk form is composed of very tiny regions, known as magnetic domains. These magnetic domains emerged from a balance of several terms viz. exchange energy, magnetocrystalline anisotropy, and magnetostatic energy [34].

Fig. 5





M–H plot of cobalt ferrite nanoparticles recorded at 300 K

The exchange energy makes an attempts to bring into line all magnetic moments in the similar direction, the magnetocrystalline anisotropy strives to orient magnetic moments along precise directions, and the magnetostatic energy seeks to abolish the magnetization in the material. In every domain, the magnetic moments of atoms are united in the single direction giving a net magnetization of all domains [35]. Hence, the net magnetization of a magnetic material originated from the addition of the different magnetizations of all magnetic domains [36]. It was found that the magnetic domains in ferromagnetic materials having very small size (less than 100 nm) below which the ferromagnetic material cannot split up further into domains and are called single or mono-domain particles [37].

Thermal energy plays an important role in the magnetic volatility of mono-domain magnetic particles. The CoFe<sub>2</sub>O<sub>4</sub> might be composed of a mono-domain, under the critical limit of its size. It might also show a superparamagnetic nature above a specific temperature which is called as the blocking temperature ( $T_B$ ) [38]. In the superparamagnetic form, the magnetic moments of the nanoparticles vary around the axes of magnetization. Thus, each one of the CoFe<sub>2</sub>O<sub>4</sub> possesses a large magnetic moment that continuously changes its orientation [39]. When an external magnetic field is applied, CoFe<sub>2</sub>O<sub>4</sub> in the superparamagnetic form shows a quick response to the changing magnetic field along with less remanent magnetization and smaller coercivity. Thus, in the superparamagnetic form, CoFe<sub>2</sub>O<sub>4</sub> nanoparticles act as a

paramagnetic atom with a giant spin [40, 41].

The magnetic parameters like saturation magnetization ( $M_s$ ), remanence magnetization ( $M_R$ ), and coercivity ( $H_c$ ) were obtained from  $M-H$  plot as 78.30 and 25.75 emu/gm and 149.86 Oe, respectively. On comparing obtained values of magnetic parameters with CoFe<sub>2</sub>O<sub>4</sub> nanoparticles prepared using sol-gel auto combustion technique [42], it is found that the presently investigated material is superior. As cobalt ferrite nanoparticles prepared by sol-gel auto combustion technique exhibit 60.50 and 36 emu/gm and 1305-Oe saturation magnetization, remanence magnetization, and coercivity, respectively. It can be explained by the smaller particle size of the present sample. As particle size decreases, the saturation and remanence magnetization enhances and coercivity decreases. The magnetic behavior of present CoFe<sub>2</sub>O<sub>4</sub> nanoparticles can be explained by Neel's ferrimagnetism model [43]. Using Neel's model the theoretical magneton number of CoFe<sub>2</sub>O<sub>4</sub> nanoparticles was calculated as

$$\eta_{\{B\}} = M_{\{B\}} - M_{\{A\}}$$

(1)

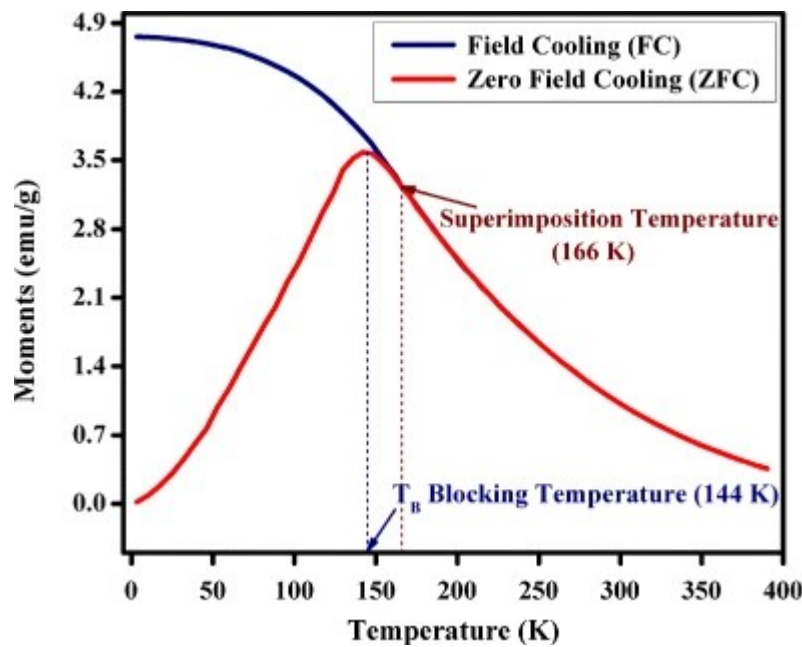
where  $M_B$  and  $M_A$  are the magnetic moments of octahedral and tetrahedral sites, respectively. It is a well-known fact that the Co<sup>2+</sup> has a preference to octahedral B sites and Fe<sup>3+</sup> occupies each tetrahedral site as well as the octahedral site [29]. However, Co<sup>2+</sup> ions have octahedral site preference it must occupy tetrahedral A sites. As cobalt ions have magnetic moment  $3 \mu_B$  and Fe<sup>3+</sup> ions as  $5 \mu_B$ . Co<sup>2+</sup> ions occupy A site by replacing Fe<sup>3+</sup> ions thereby decreasing the magnetic moment of A sites. Thus, net magnetic moment increases with Co<sup>2+</sup> ions. The experimental magneton number obtained was  $3.28 \mu_B$  and that of calculated using Neel's model was  $3.4 \mu_B$ . This indicates that Co<sup>2+</sup> ions partially occupied tetrahedral A sites. The resulting cation distribution can be written as (Co<sub>0.1</sub>Fe<sub>0.9</sub>)<sup>A</sup> (Co<sub>0.9</sub>Fe<sub>1.1</sub>)<sup>B</sup>. Similar cation distribution as (Co<sub>0.095</sub>Fe<sub>0.905</sub>)<sup>A</sup> (Co<sub>0.905</sub>Fe<sub>1.095</sub>)<sup>B</sup> was deduced from XRD pattern of the presently investigated sample. Thus, it is well-supported and confirmed the Co<sup>2+</sup> ions distribution over both sub-lattices.

### 3.1.4 Low-Temperature Magnetization

Thermal behavior of nanoparticles is studied for the confirmation of superparamagnetism and

to study the effect of temperature on magnetic properties. The commonly used technique for the investigation of superparamagnetic relaxation is the field-cooled (FC) and zero-field-cooled (ZFC) magnetization, that is, the magnetization in a weak applied field as a function of increasing temperature after the sample has been cooled, respectively, in the presence and absence of a weak magnetic field [44, 45]. Figure 6 shows the temperature-dependent ZFC and FC curves for the sample.

Fig. 6



Zero-field cooling (ZFC) and field-cooling (FC) curve of the cobalt ferrite nanoparticles

Generally, from the graph, it can be seen from the ZFC measurements the CoFe<sub>2</sub>O<sub>4</sub> was cooled from room to a low temperature in the absence of magnetic field. Then, a small magnetic field (about 100 Oe) is applied and the magnetization is measured as the temperature was being raised. As temperature increases, thermal energy will cause the moments to align along the direction of the applied magnetic field. The number of these aligned moments will increase as the temperature increases reaching a maximum at  $T_B$  [46]. As the temperature is raised above  $T_B$ , the thermal energy becomes large enough to cause the magnetic moments to flip randomly which results in a suppression of the magnetization of the particle. The ZFC curve reached a maximum at 144 K for CoFe<sub>2</sub>O<sub>4</sub> and this is considered as the blocking temperature of

the sample ( $T_B$ ). At temperatures below the blocking temperature, the thermal agitation becomes small and will not be able to cause fluctuations in the orientations of the magnetic moments of the nanoparticles where they freeze in random orientations. Hence, the CoFe<sub>2</sub>O<sub>4</sub> sample shows superparamagnetic nature [47, 48]. However, the superimposition of FC-ZFC takes place at 166 K for CoFe<sub>2</sub>O<sub>4</sub> sample. The superimposition of FC-ZFC curves is the typical characteristic feature of the superparamagnetic system [49, 50]. The superparamagnetism is induced in the system when the system's transfer from multi-domain to single and uniformly magnetized domains. The overall system is then in a state of uniform magnetization and its phase transition occurs from and ferromagnetic to superparamagnetic [51].

In FC measurements, the CoFe<sub>2</sub>O<sub>4</sub> was cooled from room temperature to a low temperature in the existence of magnetic field. The magnetization is measured as the temperature was being cooled. At  $T > T_B$ , thermal energy was large enough to randomize the magnetic moments in the particle leading to very small net magnetization [52]. As the temperature is lowered, thermal energy decreased and for some moments, it becomes smaller than that produced by the aligning field. This causes some moments to align along the field direction leading to an increase in magnetization [53]. As the temperature decreases further, more and more moments will be frozen along the direction of the applied field. The magnetization of the CoFe<sub>2</sub>O<sub>4</sub> expected to keep increasing down to the lowest temperature in single-domain nanoparticles [54].

## 3.2 Thermophysical Investigations

### 3.2.1 Thermal Conductivity

In the present study, the thermal conductivity of the CoFe<sub>2</sub>O<sub>4</sub>-ethylene glycol nanofluids was measured by using a KD2 Pro (Decagon Devices, Inc., USA) thermal properties analyzer with a maximum error of about 5%. This device employs the transient hot wire (THW) technique to measure the thermal conductivity of nanofluid which is a fast and reliable method [55, 56]. In order to measure the thermal conductivity of the samples, a cylindrical testing chamber with a diameter of 30 mm and length of 100 mm was used. After loading nanofluids into the cylindrical testing chamber, the KD2 Pro KS-1 (stainless steel single needle) sensor, with length of 60 mm and diameter of 1.27 mm was vertically inserted into the center of nanofluids. This sensor has been especially proposed to measure the thermal conductivity of

most fluids. The needle approximates the infinite line heat source. Each measurement cycle is the 60s. Heat is applied for the 30s. Thirty seconds are allowed for temperature equilibration before heating starts. After the reading, the controller computes thermal conductivity using the change in temperature. The thermal conductivity of fluids can be obtained by the following equation:

$$k = \frac{q (\ln t_2 - \ln t_1)}{4(\Delta T_2 - \Delta T_1)}$$

(2)

where  $q$  is the constant heat rate and  $\Delta T_2$  and  $\Delta T_1$  are the changes in temperature at times  $t_2$  and  $t_1$ , respectively. It should be noted that a stable temperature bath was used to stabilize the temperature of the samples. All the measurements of the thermal conductivity were repeated three times, which the average values of repeated measurements were recorded. The interval between two single measurements was 10 min.

Figure 7 shows the variation in thermal conductivity of cobalt ferrite ethylene glycol-based nanofluid as a function of nanoparticle volume fraction at various temperatures. The thermal conductivity significantly increases with increase in nanoparticles volume fraction. A similar trend was obtained experimentally at each temperature. It demonstrates that addition of nanoparticle volume fraction improves the thermal conductivity of nanofluid. It can be explained by the higher thermal conductivity of cobalt ferrite nanoparticles than carrier liquids. The thermal conductivity of presently investigated CoFe<sub>2</sub>O<sub>4</sub> nanoparticles was 4.1 W/mK and that of ethylene glycol is 0.25 W/mK. Hence, the addition of CoFe<sub>2</sub>O<sub>4</sub> nanoparticles enhanced the thermal conductivity of nanofluid. Enhancement in thermal conductivity of nanofluid with cobalt ferrite nanoparticles can further explain by the Brownian motion [57], the creation of complexes and collisions between them, and clustering and layer formation of fluid molecules with nanoparticles surface [58]. The clustering leads to path creation with lower thermal resistance [59], which results in heat transfer enhancement in the fluid. The magnitude of clusters is a function of nanoparticle dimension and its volume fraction. Thus, this phenomenon can influence the thermal conductivity of nanofluids [60]. It is well accepted that the smaller clusters have an extensive effect on thermal conductivity of nanofluids. The higher volume fraction leads to the smaller distance between the nanoparticles; consequently,



the probability of formation of cluster attraction increases. When the clustering takes place, the active surface area to volume ratio reduces; thereby resulting thermal conductivity reduction. Thus, more volume fraction leads to moderate enhancement in the thermal conductivity. It is precisely observed from Fig. 7 that the thermal conductivity enhancement above 0.4% volume fraction is lower than that up to 0.2% volume fraction. The higher nanoparticle volume fraction may increase the average dimension of the clusters. Hence, less degree of enhancement in thermal conductivity may occur. The thermal conductivity measurements show the maximum enhancement of ~ 30% in 1% volume fraction at 80 °C. The thermal conductivity of nanofluids can be estimated by either static or dynamic model. The existing theoretical models [57], the static model nanoparticles are assumed to be motionless in the base fluid; wherein thermal conductivity is predicted by the conduction-based model. Hence, the interfacial solid-liquid nanolayer results in unique thermophysical signature by differing to that of particles or fluid. The dynamic model works on the Brownian motion which is responsible for energy transport and turned as an efficient heat-transfer mechanism. The small clusters suspended in the fluid move faster and result in better energy transport. Hence, the Brownian motion contribution enhances the thermal conductivity.

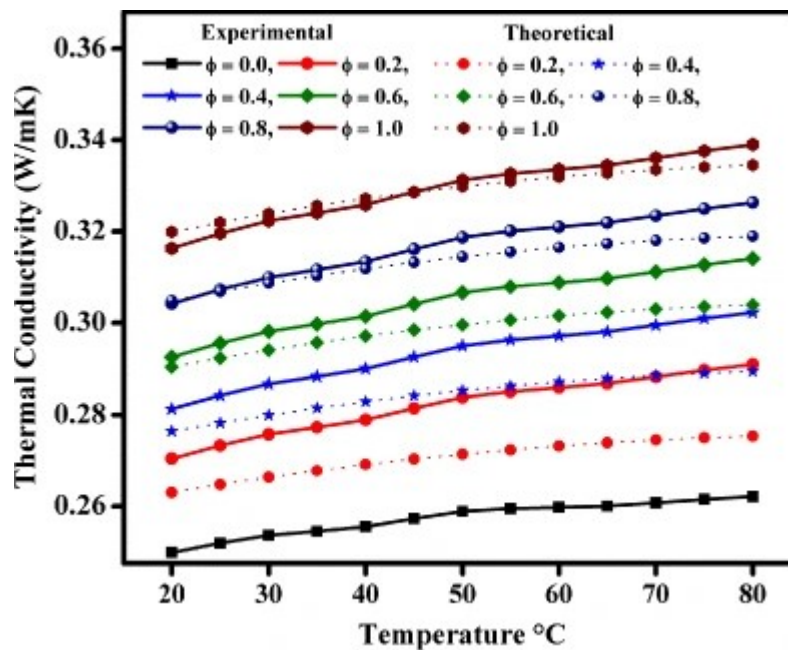
$$\frac{k_{\text{nf}}}{k_f} = \frac{k_p + 2k_f + 2\varphi(k_p + k_f)}{k_p + 2k_f + \varphi(k_p + k_f)}$$

(3)

Moreover, Fig. 7 also depicts the variations of nanofluids thermal conductivity versus temperature for various nanofluid CoFe<sub>2</sub>O<sub>4</sub>-ethylene glycol samples. Generally, it can be observed that with an increase in temperature, the thermal conductivity increases generally. The main reason of thermal conductivity enhancing due to the temperature increase can be characterized by Brownian motion, the loosening of the intermolecular bonds in the fluid layers, an increase in the number of collisions between nanoparticles; this causes the increase in interactions between the nanoparticles [56, 61]. Nanoparticle movement increases with rising temperature, and thermal conductivity improves due to a greater number of collisions between surface atoms with fluid molecules. However, the thermal conductivity of ethylene glycol considerably enhanced with increasing temperature, while the thermal conductivity of nanofluid slightly enhances. In fact, when nanoparticles are present in the ethylene glycol, the creation of nano-clusters takes place. Therefore, the Brownian motion is limited due to van

der Waals forces; as a result, the effect of temperature becomes lower [60, 62]. Temperature and volume fraction significantly affects the thermal conductivity ratio of nanofluids. From the observations, it reveals that the thermal conductivity ratio of nanofluids enhanced with increasing temperature as well as volume fraction.

Fig. 7



Variation in thermal conductivity of cobalt ferrite-ethylene glycol nanofluids with temperature

Furthermore, Fig. 7 indicates that the thermal conductivity curves of CoFe<sub>2</sub>O<sub>4</sub>-ethylene glycol nanofluid system slightly follow the theoretical curves for 0.2 and 0.4 volume fractions. However, remaining volume fraction curves closely follow theoretical curves with a minor difference.

### 3.2.2 Specific Heat Analysis

The specific heat ( $C_{nf}$ ), a thermophysical quantity, of a nanofluid is estimated based on the physical principle of the mixture rule [63] as,

$$C_{nf} = \frac{\varphi}{\rho_p} C_p + (1 - \varphi) \rho_f C_f$$

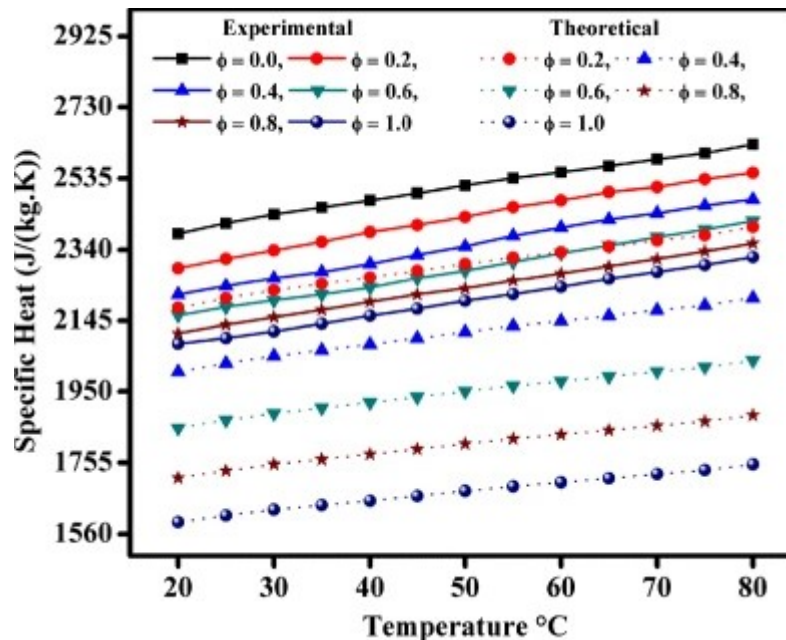
$$\{\rho_p C_p + (1 - \rho_p) \rho_f C_f\} \phi \quad (4)$$

(4)

where  $\rho_p$  is the density of nanoparticles,  $C_p$  is the specific heat of nanoparticles,  $\rho_f$  is density heat of base liquid,  $C_f$  is specific heat of base liquid, and  $\phi$  is volume fraction.

The experimentally obtained specific heat for each sample has a considerable deviation with that of theoretical value (Fig. 8). It was found to decrease with increasing volume fraction, but as a function of temperature, it increases with a rise in temperature. The observed deviation is likely due to the formation of nanolayer between the nanoparticle and the fluid. A well-known fact is that the specific heat capacity depends on the bulk phases and the nature of interfacial nanolayers. As the surface of the nanoparticles has multiple phases, the specific heat decreases with volume fraction.

Fig. 8

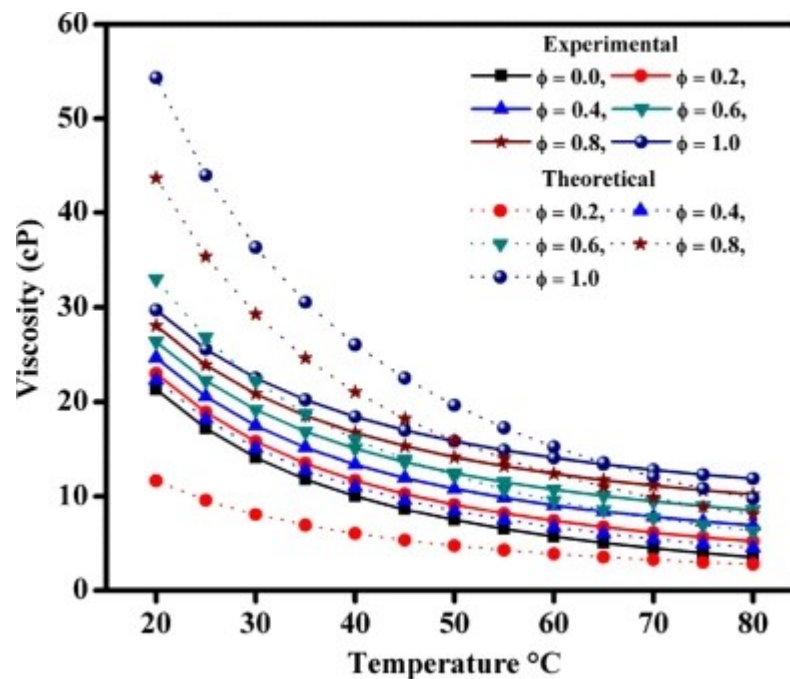


Variation in specific heat of cobalt ferrite–ethylene glycol nanofluids with temperature

### 3.2.3 Viscosity Analysis

Figure 9 shows the viscosity of the nanofluid as a function of the temperature of varying volume fraction. It reveals the increase in viscosity with increasing volume fraction from 11 to 55 cP. The viscosity plays a vital role in momentum transfer between liquid layers and withstands the relative movement of the liquid [64]. This phenomenon resulted by the Van der Waals forces between the molecules [65]. Therefore, the cobalt ferrite nanoparticles dispersion in ethylene glycol (EG) would increase the viscosity of the fluid. By increasing the number of nanoparticles in a specific amount of EG, larger nanoclusters arise due to the Van der Waals forces between them, which can prevent the movement of EG layers on each other. It may lead to improvement in viscosity of nanofluid.

Fig. 9



Variation in viscosity of cobalt ferrite–ethylene glycol nanofluids with temperature

Primarily, temperature and particle volume fraction influence the viscosity of nanofluid. The effective viscosity ( $\mu_{nf}$ ) of a suspension of solids may be written [4, 66] as:

$$\frac{\mu_{nf}}{\mu_f} = 1 + 2.5\phi$$

(5)

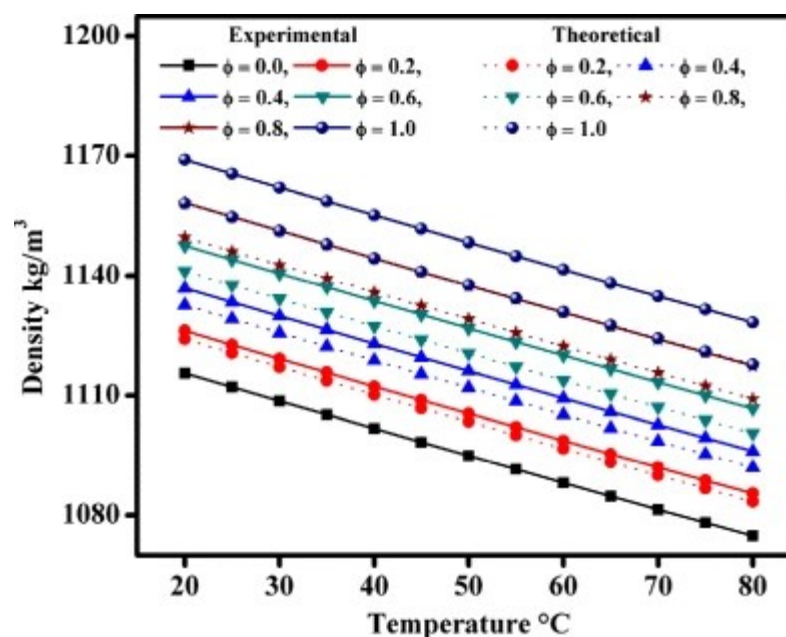
where  $\phi$  is the volume fraction of the nanoparticles and  $\mu_f$  is the viscosity of the base fluid. Both experimental and theoretical results over the temperature range 20–50 °C reduce rapidly and profoundly different from each other. Beyond 55 °C, both experimental and theoretical results show good agreement. This naturally implies that non-Newtonian corrections are essential for nanofluids such as this. Once again, the interfacial layer between the nanoparticles and fluid seem to be relevant.

It is noted from Fig. 9 that the viscosity of nanofluid reduces with the rise in temperature. As temperature increases, the intermolecular interactions between the molecules weaken and the viscosity reduces. Moreover, it is observed that the higher the volume fraction, the greater the effect of temperature viscosity. In addition to the interfacial effect pointed above, the probability of agglomeration of nanoparticles in the base fluid increases and viscosity significantly affected by volume fraction.

### 3.2.4 Density Analysis

Figure 10 shows the density of the nanofluid as a function of the temperature of varying volume fractions. The density is a significant physical property of the fluid and affects the friction factor, pump loss, and Reynolds number [67, 68]. It is directly related to particle volume fraction.

Fig. 10



## Variation in the density of cobalt ferrite–ethylene glycol nanofluids with temperature

In the present investigation as shown in Fig. 8, it rises approximately in a linear manner with volume fraction and decreases with increase in temperature. The increasing nanoparticles volume fraction and these nanoparticles were increased crowd per unit volume. It causes agglomeration, hence, the density enhancement. The enhancement in the density of CoFe<sub>2</sub>O<sub>4</sub>-ethylene glycol mainly owed to the fact of a denser nature of ethylene glycol. The theoretical model accounts for the variation of concentration at various temperatures. To determine the rheology of suspensions, volume concentration is often used instead of mass concentration. Once the particle volume concentration is determined, the density of the nanofluid ( $\rho_{nf}$ ) can be determined from,

$$\rho_{nf} = \varphi_p \rho_p + (1 - \varphi_p) \rho_f$$

(6)

where  $\rho_p$  is the density of particles,  $\rho_f$  is the density of the base liquid, and  $\varphi_p$  is the volume fraction of the particles. The decrease in density with temperature is due to the weakening of bonds at elevated temperature [69]. It can be noted that the obtained values of densities are within the range. Further, it is noted that the experimental curves follow the theoretical curves for 0.2–0.6 volume fractions. However, the theoretical curves of 0.8 and 1.0 volume fraction possess a smaller difference.

## 4 Conclusions

The single phase with Fd-3m space group CoFe<sub>2</sub>O<sub>4</sub> nanoparticles were synthesized successfully using co-precipitation technique. The morphology revealed spherical nature and some of the agglomerations. M–H loop favored the superparamagnetic nature of CoFe<sub>2</sub>O<sub>4</sub> nanoparticles. The low-temperature magnetization reveals the blocking temperature of the CoFe<sub>2</sub>O<sub>4</sub> curve is of 144 K. The stable CoFe<sub>2</sub>O<sub>4</sub>-ethylene glycol based nanofluid of varying volume fractions prepared using the ultrasonically assisted technique. The experimental

results indicated significant augmentation in thermal conductivity with both nanoparticle volume fraction and temperature. The specific heat was decreased with nanoparticles volume fractions and augmented with the rise in temperature. The viscosity showed that each sample exhibit the Newtonian behavior. The proposed correlation between thermal conductivity and the experimental results revealed high accuracy.

## Abbreviations

---

$\varphi$ : Volume fraction (%)

$\lambda$ : Wavelength of x-ray (Å)

$\chi^2$ : Goodness of fit

$a$ : Lattice constant (Å)

$\rho$ : Density (kg/m<sup>3</sup>)

$S$ : Specific surface area (m<sup>2</sup>/g)

$T_B$ : Blocking temperature (K)

$M_S$ : Saturation magnetization (emu/gm)

$M_R$ : Remanence magnetization (emu/gm)

$H_c$ : Coercivity (Oe)

$\eta_B$ : Magnetron number

$k$ : Thermal conductivity (W/mK)

$c$ : Specific heat (J/(kg K))

$\mu$ : Viscosity (cP)

$R_p, R_{wp}$ : Profile Reliability Index, Weighted Profile Reliability Index

$nf$ : Nanofluids

$p$ : Nanoparticles

$f$ : Fluid

## References

---

1. Shima, P., Philip, J.: Tuning of thermal conductivity and rheology of nanofluids using an external stimulus. *J. Phys. Chem. C* 115, 20097–20104 (2011)

[Article](#) [Google Scholar](#)

2. Rashin, M.N., Hemalatha, J.: A novel ultrasonic approach to determine thermal conductivity in CuO–ethylene glycol nanofluids. *J. Mol. Liq.* 197, 257–262 (2014)

[Article](#) [Google Scholar](#)

3. Ashraf, M.W., Tayyaba, S., Afzulpurkar, N.: Micro electromechanical systems (MEMS) based microfluidic devices for biomedical applications. *Int. J. Mol. Sci.* 12, 3648–3704 (2011)

[Article](#) [Google Scholar](#)

4. Saidur, R., Leong, K., Mohammad, H.: A review on applications and challenges of nanofluids. *Renew. Sustain. Energy Rev.* 15, 1646–1668 (2011)



[Article](#) [Google Scholar](#)

5. Philip, J., Jaykumar, T., Kalyanasundaram, P., Raj, B.: A tunable optical filter. *Meas. Sci. Technol.* 14, 1289 (2003)

[Article](#) [ADS](#) [Google Scholar](#)

6. Das, S.K., Choi, S.U., Yu, W., Pradeep, T.: *Nanofluids: science and technology*. Wiley, Hoboken (2007)

[Book](#) [Google Scholar](#)

7. Hayat, T., Waqas, M., Shehzad, S., Alsaedi, A.: A model of solar radiation and Joule heating in magnetohydrodynamic (MHD) convective flow of thixotropic nanofluid. *J. Mol. Liq.* 215, 704–710 (2016)

[Article](#) [Google Scholar](#)

8. Kale, G., Humbe, A.V., Kharat, P., Bhoyar, D., Jadhav, K.: Tartaric acid a novel fuel approach: synthesis and characterization of CoFe<sub>2</sub>O<sub>4</sub> nano particles

9. Mahadik, M.M., Kharat, P.B.: Aliphatic organic compounds: a substitute of ferrite materials in isolator for high frequency application

10. Peyghambarzadeh, S., Hashemabadi, S., Hoseini, S., Jamnani, M.S.: Experimental study of heat transfer enhancement using water/ethylene glycol based nanofluids as a new coolant for car radiators. *Int. Commun. Heat Mass Transf.* 38, 1283–1290 (2011)

[Article](#) [Google Scholar](#)

11. Zhang, X., Gu, H., Fujii, M.: Effective thermal conductivity and thermal diffusivity of nanofluids containing spherical and cylindrical nanoparticles. *Exp. Therm. Fluid Sci.* 31, 593–599 (2007)

[Article](#) [Google Scholar](#)

12. Patel, H.E., Sundararajan, T., Das, S.K.: An experimental investigation into the thermal conductivity enhancement in oxide and metallic nanofluids. *J. Nanoparticle Res.* 12, 1015–1031 (2010)

[Article](#) [ADS](#) [Google Scholar](#)

13. Pastoriza-Gallego, M.J., Lugo, L., Legido, J.L., Piñeiro, M.M.: Thermal conductivity and viscosity measurements of ethylene glycol-based Al<sub>2</sub>O<sub>3</sub> nanofluids. *Nanoscale Res. Lett.* 6, 221 (2011)

[Article](#) [ADS](#) [Google Scholar](#)

14. Pastoriza-Gallego, M.J., Lugo, L., Legido, J.L., Piñeiro, M.M.: Rheological non-Newtonian behaviour of ethylene glycol-based Fe<sub>2</sub>O<sub>3</sub> nanofluids. *Nanoscale Res. Lett.* 6, 560 (2011)

[Article](#) [ADS](#) [Google Scholar](#)

15. Zhu, H., Zhang, C., Liu, S., Tang, Y., Yin, Y.: Effects of nanoparticle clustering and alignment on thermal conductivities of Fe<sub>3</sub>O<sub>4</sub> aqueous nanofluids. *Appl. Phys. Lett.* 89, 023123 (2006)

[Article](#) [ADS](#) [Google Scholar](#)

16. Abareshi, M., Goharshadi, E.K., Zebarjad, S.M., Fadafan, H.K., Youssefi, A.: Fabrication, characterization and measurement of thermal conductivity of Fe<sub>3</sub>O<sub>4</sub> nanofluids. *J. Magn. Magn. Mater.* 322, 3895–3901 (2010)

[Article](#) [ADS](#) [Google Scholar](#)

17. Sundar, L.S., Singh, M.K., Sousa, A.C.: Investigation of thermal conductivity and viscosity of Fe<sub>3</sub>O<sub>4</sub> nanofluid for heat transfer applications. *Int. Commun. Heat Mass Transf.* 44, 7–14 (2013)

[Article](#) [Google Scholar](#)

18. Sundar, L.S., Singh, M.K., Sousa, A.C.: Thermal conductivity of ethylene glycol and water mixture based Fe<sub>3</sub>O<sub>4</sub> nanofluid. *Int. Commun. Heat Mass Transf.* 49, 17–24 (2013)

[Article](#) [Google Scholar](#)

19. Bahiraei, M., Hangi, M.: An empirical study to develop temperature-dependent models for thermal conductivity and viscosity of water–Fe<sub>3</sub>O<sub>4</sub> magnetic nanofluid. *Mater. Chem. Phys.* 181, 333–343 (2016)

[Article](#) [Google Scholar](#)

20. Bahiraei, M.: Effect of particle migration on flow and heat transfer characteristics of magnetic nanoparticle suspensions. *J. Mol. Liq.* 209, 531–538 (2015)

[Article](#) [Google Scholar](#)

21. Sheikholeslami, M., Hatami, M., Ganji, D.: Nanofluid flow and heat transfer in a rotating system in the presence of a magnetic field. *J. Mol. Liq.* 190, 112–120 (2014)

[Article](#) [Google Scholar](#)

22. Mohebbi, A.: Prediction of specific heat and thermal conductivity of nanofluids by a combined equilibrium and non-equilibrium molecular dynamics simulation. *J. Mol. Liq.* 175, 51–58 (2012)

[Article](#) [Google Scholar](#)

23. Kharat, P.B., Shisode, M., Birajdar, S., Bhoyar, D., Jadhav, K.: Synthesis and characterization of water based NiFe<sub>2</sub>O<sub>4</sub> ferrofluid. In: AIP Conference Proceedings, p 050122. AIP Publishing (2017)
24. Kharat, P.B., Kounsalye, J.S., Humbe, A.V., Birajdar, S.D., Jadhav, K.: Preparation and diverse properties of cobalt ferrite ferrofluid
25. Kounsalye, J.S., Kharat, P.B., Chavan, A.R., Humbe, A.V., Borade, R., Jadhav, K.: Symmetry transition via tetravalent impurity and investigations on magnetic properties of Li<sub>0.5</sub>Fe<sub>2.5</sub>O<sub>4</sub>. In: AIP Conference Proceedings, p 050067. AIP Publishing (2018)
26. Kounsalye, J.S., Kharat, P.B., Bhoyar, D.N., Jadhav, K.: Radiation-induced modifications in structural, electrical and dielectric properties of Ti<sup>4+</sup> ions substituted Li<sub>0.5</sub>Fe<sub>2.5</sub>O<sub>4</sub> nanoparticles. J. Mater. Sci. Mater. Electron. 29(10):8601–8609
27. Kounsalye, J.S., Kharat, P.B., Shisode, M.V., Jadhav, K.: Influence of Ti<sup>4+</sup> ion substitution on structural, electrical and dielectric properties of Li<sub>0.5</sub>Fe<sub>2.5</sub>O<sub>4</sub> nanoparticles. J. Mater. Sci. Mater. Electron. 28, 17254–17261 (2017)

[Article](#) [Google Scholar](#)

28. Chavan, A.R., Chilwar, R.R., Kharat, P.B., Jadhav, K.: Effect of annealing temperature on structural, morphological, optical and magnetic properties of NiFe<sub>2</sub>O<sub>4</sub> thin films. J. Supercond. Nov. Magn. (2018). <https://doi.org/10.1007/s10948-018-4565-3>
29. Humbe, A.V., Kharat, P.B., Nawle, A.C., Jadhav, K.: Nanocrystalline Ni<sub>0.70-x</sub>Cu<sub>x</sub>Zn<sub>0.30</sub>Fe<sub>2</sub>O<sub>4</sub> with 0 ≤ x ≤ 0.25 prepared by nitrate-citrate route: structure, morphology and

electrical investigations. *J. Mater. Sci. Mater. Electron.* 29, 3467–3481 (2018)

[Article](#) [Google Scholar](#)

30. Alam, R.S., Moradi, M., Rostami, M., Nikmanesh, H., Moayedi, R., Bai, Y.: Structural, magnetic and microwave absorption properties of doped Ba-hexaferrite nanoparticles synthesized by co-precipitation method. *J. Magn. Magn. Mater.* 381, 1–9 (2015)

[Article](#) [ADS](#) [Google Scholar](#)

31. Shanmugavani, A., Selvan, R.K., Layek, S., Vasylechko, L., Sanjeeviraja, C.: Influence of pH and fuels on the combustion synthesis, structural, morphological, electrical and magnetic properties of CoFe<sub>2</sub>O<sub>4</sub> nanoparticles. *Mater. Res. Bull.* 71, 122–132 (2015)

[Article](#) [Google Scholar](#)

32. Humbe, A.V., Nawle, A.C., Shinde, A., Jadhav, K.: Impact of Jahn Teller ion on magnetic and semiconducting behaviour of Ni-Zn spinel ferrite synthesized by nitrate-citrate route. *J. Alloys Compd.* 691, 343–354 (2017)

[Article](#) [Google Scholar](#)

33. Obaidat, I.M., Issa, B., Haik, Y.: Magnetic properties of magnetic nanoparticles for efficient hyperthermia. *Nanomaterials* 5, 63–89 (2015)

[Article](#) [Google Scholar](#)

34. Tumanski, S.: *Handbook of magnetic measurements*. CRC Press, Boca Raton (2016)

[Google Scholar](#)

35. Yadav, R.: *Synthesis and characterization of structural and magnetic properties of*

electrodeposited cobalt iron thin film. In: Indian Institute of Technology Hyderabad (2015)

36. Yu, G., Upadhyaya, P., Fan, Y., Alzate, J.G., Jiang, W., Wong, K.L., Takei, S., Bender, S.A., Chang, L.-T., Jiang, Y.: Switching of perpendicular magnetization by spin–orbit torques in the absence of external magnetic fields. *Nat. Nanotechnol.* 9, 548 (2014)

[Article](#) [ADS](#) [Google Scholar](#)

37. Srdić, V.V., Cvejić, Z., Milanović, M., Stojanović, G., Rakić, S.: Metal oxide structure, crystal chemistry, and magnetic properties. In: *Magnetic, Ferroelectric, and Multiferroic Metal Oxides*, pp 313–332. Elsevier (2018)

38. Kolen'ko, Y.V., Banñobre-Loópez, M., Rodríguez-abreu, C., Carboó-Argibay, E., Sailsman, A., Pinñeiro-Redondo, Y., Cerqueira, M.F., Petrovykh, D.Y., Kovnir, K., Lebedev, O.I.: Large-scale synthesis of colloidal Fe<sub>3</sub>O<sub>4</sub> nanoparticles exhibiting high heating efficiency in magnetic hyperthermia. *J. Phys. Chem. C* 118, 8691–8701 (2014)

[Article](#) [Google Scholar](#)

39. Gonçalves, E., Cornejo, D., Oliveira, C., Neto, A.F., Depeyrot, J., Tourinho, F., Aquino, R.: Magnetic and structural study of electric double-layered ferrofluid with MnFe<sub>2</sub>O<sub>4</sub>@ $\gamma$ -Fe<sub>2</sub>O<sub>3</sub> nanoparticles of different mean diameters: determination of the magnetic correlation distance. *Phys. Rev. E* 91, 042317 (2015)

[Article](#) [ADS](#) [Google Scholar](#)

40. Sharma, S.K.: Exchange bias: from thin film to nanogranular and bulk systems. CRC Press, Boca Raton (2017)

[Book](#) [Google Scholar](#)

41. Zhang, S., Zhao, D.: Advances in magnetic materials: processing, properties, and performance. CRC Press, Boca Raton (2017)

[Book](#) [Google Scholar](#)

42. Gharibshahian, M., Mirzaee, O., Nourbakhsh, M.: Evaluation of superparamagnetic and biocompatible properties of mesoporous silica coated cobalt ferrite nanoparticles synthesized via microwave modified Pechini method. *J. Magn. Magn. Mater.* 425, 48–56 (2017)

[Article](#) [Google Scholar](#)

43. Humbe, A.V., Kounsalye, J.S., Shisode, M.V., Jadhav, K.: Rietveld refinement, morphology and superparamagnetism of nanocrystalline Ni<sub>0.70-x</sub> Cu<sub>x</sub> Zn<sub>0.30</sub> Fe<sub>2</sub> O<sub>4</sub> spinel ferrite, *Ceramics International* (2017)

44. Khot, V., Salunkhe, A., Ruso, J., Pawar, S.: Improved magnetic induction heating of nanoferrites for hyperthermia applications: correlation with colloidal stability and magneto-structural properties. *J. Magn. Magn. Mater.* 384, 335–343 (2015)

[Article](#) [ADS](#) [Google Scholar](#)

45. Kandasamy, G., Maity, D.: Recent advances in superparamagnetic iron oxide nanoparticles (SPIONs) for in vitro and in vivo cancer nanotheranostics. *Int. J. Pharm.* 496, 191–218 (2015)

[Article](#) [Google Scholar](#)

46. Khot, V., Salunkhe, A., Thorat, N., Ningthoujam, R., Pawar, S.: Induction heating studies of dextran coated MgFe<sub>2</sub> O<sub>4</sub> nanoparticles for magnetic hyperthermia. *Dalton Trans.* 42, 1249–1258 (2013)

[Article](#) [Google Scholar](#)

47. Koksharov, Y.A.: Magnetism of nanoparticles: effects of size, shape, and interactions. *Magnetic nanoparticles:2011* (2009)
48. Salunkhe, A., Khot, V., Phadatare, M., Thorat, N., Joshi, R., Yadav, H., Pawar, S.: Low temperature combustion synthesis and magnetostructural properties of Co–Mn nanoferrites. *J. Magn. Magn. Mater.* 352, 91–98 (2014)

[Article](#) [ADS](#) [Google Scholar](#)

49. Leufke, P.M.: Magnetolectric coupling in layered LSMO/PZT nanostructures, In: *Technische universität* (2014)
50. Nikam, D., Jadhav, S., Khot, V., Phadatare, M., Pawar, S.: Study of AC magnetic heating characteristics of Co<sub>0.5</sub>Zn<sub>0.5</sub>Fe<sub>2</sub>O<sub>4</sub> nanoparticles for magnetic hyperthermia therapy. *J. Magn. Magn. Mater.* 349, 208–213 (2014)

[Article](#) [ADS](#) [Google Scholar](#)

51. Rosensweig, R.E.: *Ferrohydrodynamics*, Courier Corporation (2013)
52. Bhuiya, A.W.: *Temperature-induced phenomena in systems of magnetic nanoparticles*. The University of Texas at El Paso (2009)
53. Issa, B., Obaidat, I.M., Albiss, B.A., Haik, Y.: Magnetic nanoparticles: surface effects and properties related to biomedicine applications. *Int. J. Mol. Sci.* 14, 21266–21305 (2013)

[Article](#) [Google Scholar](#)



54. Evans, M., Heller, F.: Environmental magnetism: principles and applications of enviromagnetics. Academic Press, Cambridge (2003)

[Google Scholar](#)

55. Manimaran, R., Palaniradja, K., Alagumurthi, N., Sendhilnathan, S., Hussain, J.: Preparation and characterization of copper oxide nanofluid for heat transfer applications. *Appl. Nanosci.* 4, 163–167 (2014)

[Article](#) [ADS](#) [Google Scholar](#)

56. Paul, G., Chopkar, M., Manna, I., Das, P.: Techniques for measuring the thermal conductivity of nanofluids: a review. *Renew. Sustain. Energy Rev.* 14, 1913–1924 (2010)

[Article](#) [Google Scholar](#)

57. Leong, K., Ahmad, K.K., Ong, H.C., Ghazali, M., Baharum, A.: Synthesis and thermal conductivity characteristic of hybrid nanofluids—a review. *Renew. Sustain. Energy Rev.* 75, 868–878 (2017)

[Article](#) [Google Scholar](#)

58. Yu, W., Xie, H.: A review on nanofluids: preparation, stability mechanisms, and applications. *J. Nanomater.* 2012, 1 (2012)

[Google Scholar](#)

59. Karthikeyan, N., Philip, J., Raj, B.: Effect of clustering on the thermal conductivity of nanofluids. *Mater. Chem. Phys.* 109, 50–55 (2008)

[Article](#) [Google Scholar](#)

60. Afrand, M.: Experimental study on thermal conductivity of ethylene glycol containing hybrid nano-additives and development of a new correlation. *Appl. Therm. Eng.* 110, 1111–1119 (2017)

[Article](#) [Google Scholar](#)

61. Toghraie, D., Chaharsoghi, V.A., Afrand, M.: Measurement of thermal conductivity of zno–tio<sub>2</sub>/EG hybrid nanofluid. *J. Therm. Anal. Calorim.* 125, 527–535 (2016)

[Article](#) [Google Scholar](#)

62. Esfe, M.H., Karimipour, A., Yan, W.-M., Akbari, M., Safaei, M.R., Dahari, M.: Experimental study on thermal conductivity of ethylene glycol based nanofluids containing Al<sub>2</sub>O<sub>3</sub> nanoparticles. *Int. J. Heat Mass Transf.* 88, 728–734 (2015)

[Article](#) [Google Scholar](#)

63. Gupta, A.K., Mishra, G., Nirmalkar, N., Chhabra, R.: Effect of confinement on heat transfer in aqueous nanofluids from a heated sphere. *Powder Technol.* 325, 576–596 (2018)

[Article](#) [Google Scholar](#)

64. Dardan, E., Afrand, M., Isfahani, A.M.: Effect of suspending hybrid nano-additives on rheological behavior of engine oil and pumping power. *Appl. Therm. Eng.* 109, 524–534 (2016)

[Article](#) [Google Scholar](#)

65. Kharat, P.B., Somvanshi, S.B., Kounsalye, J.S., Deshmukh, S.S., Khirade, P.P., Jadhav, K.: Temperature dependent viscosity of cobalt ferrite/ethylene glycol ferrofluids. In: AIP Conference Proceedings, p 050044. AIP Publishing (2018)
66. Wu, J., Zhao, J.: A review of nanofluid heat transfer and critical heat flux enhancement—research gap to engineering application. *Prog. Nucl. Energy* 66, 13–24 (2013)
- [Article](#) [Google Scholar](#)
67. Kandlikar, S., Garimella, S., Li, D., Colin, S., King, M.R.: Heat transfer and fluid flow in minichannels and microchannels. Elsevier, NY (2005)
- [Google Scholar](#)
68. Faghri, A.: Heat pipe science and technology. Global Digital Press, Kanpur (1995)
- [Google Scholar](#)
69. Suganthi, K.S., Anusha, N., Rajan, K.S.: Low viscous ZnO–propylene glycol nanofluid: a potential coolant candidate. *J. Nanoparticle Res.* 15, 1986 (2013)

[Article](#) [ADS](#) [Google Scholar](#)

## Acknowledgments

---

The authors are thankful to Professor John Philip, Indira Gandhi Center for Atomic Research Center, Kalpakkam, Tamilnadu, as well as Professor J. B. Naik, Head, University Institute of Chemical Technology, North Maharashtra University, Jalgaon, Maharashtra, for providing thermal conductivity and specific heat measurement facilities.

## Author information

---

### Authors and Affiliations

Department of Physics, Dr. Babasaheb Ambedkar Marathwada University, Aurangabad, Maharashtra, 431001, India

Prashant B. Kharat, Jitendra S. Kounsalye, Mahendra V. Shisode & K. M. Jadhav

### Corresponding author

Correspondence to [Prashant B. Kharat](#).

## Rights and permissions

---

[Reprints and permissions](#)

## About this article

---

### Cite this article

Kharat, P.B., Kounsalye, J.S., Shisode, M.V. *et al.* Preparation and Thermophysical Investigations of CoFe<sub>2</sub>O<sub>4</sub>-based Nanofluid: a Potential Heat Transfer Agent. *J Supercond Nov Magn* 32, 341–351 (2019). <https://doi.org/10.1007/s10948-018-4711-y>

Received

12 April 2018

Accepted

25 April 2018

Published

11 May 2018

Issue Date

February 2019

DOI

<https://doi.org/10.1007/s10948-018-4711-y>

### Share this article

Anyone you share the following link with will be able to read this content:

[Get shareable link](#)

Provided by the Springer Nature SharedIt content-sharing initiative

## Keywords

[CoFe<sub>2</sub>O<sub>4</sub> nanoparticles](#)

[Nanofluids](#)

[Ethylene glycol](#)

[Volume fraction](#)

[Temperature](#)